Solution of Three-Dimensional Reference Interaction Site Model and Hypernetted Chain Equations for Simple Point Charge Water by Modified Method of Direct Inversion in Iterative Subspace

ANDRIY KOVALENKO,* SEIICHIRO TEN-NO, FUMIO HIRATA
Institute for Molecular Science, Myodaiji, Okazaki, Aichi 444-8585, Japan

Received 31 August 1998; accepted 1 February 1999

ABSTRACT: We proposed a modified procedure of the direct inversion in the iterative subspace (DIIS) method to accelerate convergence in the integral equation theory of liquids. We update the DIIS basis vectors at each iterative step by using the approximate residual obtained in the DIIS extrapolation. The procedure is tested by solving the 3-dimensional (3-D) generalization of the reference interaction site model equation together with the hypernetted chain closure, as well as their 1-D version. We calculated the 3-D site distribution of water, represented by the simple point charge model, around one water molecule considered as a central particle. © 1999 John Wiley & Sons, Inc. J Comput Chem 20: 928–936, 1999

Keywords: water; reference interaction site model; hypernetted chain closure; 3-dimensional site profiles; direct inversion in iterative subspace

Introduction

Theoretical calculation of liquid structure requires solving an integral equation for distribution functions of the liquid. It is common to employ the Ornstein–Zernike (OZ) equation for the binary distribution functions, complemented with so-called closure relations that are in general nonlinear.[1] In the case of a molecular liquid the distribution functions depend on molecular orientations as well as separations, and the OZ equation becomes 6-dimensional (6-D). By averaging the pair distribution functions over orientations, it is reduced to the reference interaction site model (RISM) equation that yields radial site–site pair

* *Permanent address:* Institute for Condensed Matter Physics, Svientsitsky Str. 1, Lviv 290011, Ukraine
Correspondence to: F. Hirata; e-mail: hirata@ims.ac.jp

CCC 0192-8651 / 99 / 090928-09

distribution functions dependent on separations between atomic sites constituting molecular particles.[2–5] Partial reduction of the initial 6-D OZ equation gives the 3-D generalization of the RISM equation, producing more detailed 3-D distribution profiles of molecular sites of liquid particles around one molecule regarded as a central particle.[6,7]

The distribution functions are usually specified on a grid, and the convolution in the OZ equation is performed by employing the fast Fourier transform (FFT). This reduces the OZ equation together with the closure relation to a set of nonlinear algebraic equations. Methods for solving the equations can be classified as direct or iterative. Direct methods execute in a predictable number of operations and provide a quadratic convergence in the region close enough to the solution. However, they cannot be readily applied because this requires calculating and inverting the Jacobian matrix, which is prohibitively wasteful for a large number of grid points. Iterative methods do not share this deficiency and are very simple to implement. At the same time, a great shortcoming is their slow convergence. This becomes of vital importance for time-consuming 3-D calculations.

Essential acceleration is achieved by replacing the Picard iteration with dynamic relaxation or evaluation of fictitious dynamics of the trial vector relaxing to the solution under the action of the equation residual.[7] This procedure is related to the Carr–Parrinello molecular dynamics method or simulated annealing.[8] The convergence rate appears to be the highest at the beginning of the process and later on slows down, nevertheless remaining significantly faster than plain iterations.

Rapidly convergent and highly efficient algorithms were devised for solving the OZ and RISM equations on a 1-D grid, which consists of expanding the solution into a few basic functions recapitulating its general behavior, calculating the expansion coefficients by the Newton–Raphson method, and then refining the solution by Picard iteration.[9–12] However, they become very difficult to use in the 3-D case, because an estimated increase of the number of coarse functions required is a third power of that necessary for a 1-D grid.

Another combination of a direct and iterative method, referred to as direct inversion in the iterative subspace (DIIS), was developed in the context of *ab initio* molecular orbital calculations.[13–15] Its essence consists of minimizing the residual in the subspace spanned by the consecutive iterated vectors, which serve as basis functions approximating the solution at the current stage of the iterational process. The basis vectors are then being updated after several conventional self-consistent field (SCF) cycles[13] or by using the approximate Fock matrix.[14,15] DIIS greatly improves convergence, especially closer to the terminal iterative steps. However, it often wastes time in the early stages of the iterational procedure outside the region of quadratic convergence.

An algorithm similar to the DIIS method with three basis vectors was used for solution of the OZ equation in a charged system.[16] The DIIS procedure updated by Picard iterations was applied to solve the RISM equations combined with the SCF calculations.[17] Recently it was proposed to update the DIIS vectors by the modified Broyden (MB) method, which is a multidimensional secant method.[18] This significantly improves convergence as compared to the pure MB method.

The present work proposes a modified DIIS method that updates the basis vectors at every iteration by using the approximate residual obtained in the DIIS extrapolation. Owing to the appropriate initial guess of the correlation function,[7] we avoid the procedures of gradual cooling and charging used in ref. 18 and start iteration at once from a given temperature and full molecular charges. We applied the method to solution of the 3-D generalization, as well as the 1-D version of the RISM and hypernetted chain (HNC) equations for liquid of strongly polar water molecules.

Modified DIIS Method

Consider a set of nonlinear equations

$$R_\gamma\left[f_1(\mathbf{r}),\ldots,f_\mu(\mathbf{r})\right]=0,\quad \gamma=1,\ldots,\mu, \qquad (1)$$

for functions $f_\gamma(\mathbf{r})$ specified on a grid of points $\mathbf{r}=\{\mathbf{r}_i\}$, $i=1,\ldots,n$.

Because an iterative procedure has been set up and m vectors $f_\gamma^{(1)}(\mathbf{r}),\ldots,f_\gamma^{(m)}(\mathbf{r})$ have been obtained in the course of iteration, a much better approximation to the solution can be constructed as their linear combination,

$$f_\gamma^{(*)}(\mathbf{r})=\sum_{j=1}^{m} c_j f_\gamma^{(j)}(\mathbf{r}), \qquad (2)$$

by requiring that the corresponding linear combination of the residual vectors,

$$R_\gamma^{(*)}(\mathbf{r}) = \sum_{j=1}^{m} c_j R_\gamma^{(j)}(\mathbf{r}), \tag{3}$$

approximates the zero vector in the mean square sense, subject to the additional condition

$$\sum_{j=1}^{m} c_j = 1. \tag{4}$$

The latter defines an $(m-1)$-dimensional plane passing through m points specifying the basis residual vectors [which linearizes eq. (1)]. This leads to the system of $m+1$ linear equations for the expansion coefficients,

$$\begin{pmatrix} S_{11} & \cdots & S_{1m} & -1 \\ \vdots & & \vdots & \vdots \\ S_{m1} & \cdots & S_{mm} & -1 \\ -1 & \cdots & -1 & 0 \end{pmatrix} \begin{pmatrix} c_1 \\ \vdots \\ c_m \\ \lambda \end{pmatrix} = \begin{pmatrix} 0 \\ \vdots \\ 0 \\ -1 \end{pmatrix}, \tag{5}$$

where $S_{jk} = \langle \mathbf{R}^{(j)} | \mathbf{R}^{(k)} \rangle$ is a scalar product of the residual vectors, defined on the grid as

$$S_{jk} = \sum_{\gamma=1}^{\mu} \sum_{i=1}^{n} R_\gamma^{(j)}(\mathbf{r}_i) R_\gamma^{(k)}(\mathbf{r}_i),$$

and λ is a Lagrangian multiplier yielding the squared norm of the minimized residual (3).

On the DIIS minimization, further improvement is possible only after updating the iterative subspace of $f_\gamma^{(j)}(\mathbf{r})$ with new vectors introducing new dimensions, which cannot be reduced to a linear combination of the previous ones. They can be obtained by performing several Picard iteration from the point of the minimized residual and then repeating the DIIS procedure.[13]

Instead, it makes sense to update the vectors at every iteration by using the residual at its extrapolated minimum. This would require two evaluations of the residual: at the minimum, $\mathbf{R}[\mathbf{f}^{(*)}]$, and at the next point, $\mathbf{R}[\mathbf{f}^{(m+1)}]$. However, similar to the SCF calculations,[14,15] the true residual at the minimum can be replaced by its DIIS extrapolation. The extrapolated residual (3) is orthogonal to the DIIS subspace, that is, to the $(m-1)$-dimensional plane passing through the points specifying the basis residuals. Therefore, (3) is a reasonable guess of the direction of further search. The next DIIS minimization introduces a gradient correction to the direction (3) since DIIS is very close to conjugate-gradient type methods.[15] Thus, we define the next iterated vector as

$$f_\gamma^{(m+1)}(\mathbf{r}_i) = f_\gamma^{(*)}(\mathbf{r}_i) + \eta R_\gamma^{(*)}(\mathbf{r}_i), \tag{6}$$

where the vector and residual at the DIIS extrapolated minimum, $f^{(*)}(\mathbf{r}_i)$ and $R^{(*)}(\mathbf{r}_i)$, are given by eqs. (2) and (3), and η is the damping parameter to be adjusted for the best convergence. This will be referred to as the modified DIIS (MDIIS) method. The procedure starts with one vector, sequentially incrementing the DIIS matrix size up to $m \times m$, and thereafter discards the earlier vectors.

The optimal value of the MDIIS damping parameter, η, is determined for a given system by a particular ratio between the scales of the residual functions, $R_\gamma(\mathbf{r}_i)$, and their arguments, $f_\gamma(\mathbf{r}_i)$. To better linearize $R_\gamma(\mathbf{r}_i)$ in the region of the next iteration, it is desirable to provide the updating term $\eta R_\gamma^{(*)}$ in (6) such that the corresponding change $R_\gamma^{(m+1)} - R_\gamma^{(*)}$ is close in magnitude to the minimized residual $R_\gamma^{(*)}$. However, in the region of quadratic convergence the effect of the parameter η decreases because for a linear functional dependence, η in fact cancels out in eq. (5).

It should be emphasized that outside a quadratic region the root mean square value of the residual,

$$\overline{R}^{(j)} = \left(\frac{1}{\mu n} \sum_{\gamma=1}^{\mu} \sum_{i=1}^{n} \left(R_\gamma^{(j)}(r_i) \right)^2 \right)^{1/2},$$

does not necessarily decrease monotonically with iterations. The residual at the new vector, which is even somewhat larger than the previous one, updates and improves the representation of the residual function (1) by the DIIS vectors. Therefore, such a rise is usually followed by a substantial drop of the residual magnitude at the next steps. However, if the root mean square residual calculated at the next point (6) appears to be essentially larger than the smallest value of those for the DIIS vectors,

$$\overline{R}^{(m+1)} > K_r \min(\overline{R}^{(1)}, \ldots, \overline{R}^{(m)}), \tag{7}$$

it is worthwhile to restart the MDIIS procedure from the point of the smallest residual because the old DIIS vectors no longer model the behavior of the residual function (1) properly. A reasonable value of the restarting threshold is one order of magnitude, $K_r = 10$. The procedure should also

be restarted if the matrix in eq. (5) becomes ill conditioned.

The next DIIS minimization introduces a gradient correction to the direction (3) since DIIS is very close to conjugate-gradient type methods.[15]

1-D RISM and HNC Equations

The conventional RISM equation for a one-component molecular liquid has the form[3–5]

$$h_{\alpha\gamma}(r_{\alpha\gamma}) = \omega_{\alpha\mu}(r_{\alpha\mu}) \otimes c_{\mu\nu}(r_{\mu\nu}) \otimes \omega_{\nu\gamma}(r_{\nu\gamma}) + \omega_{\alpha\mu}(r_{\alpha\mu}) \otimes c_{\mu\nu}(r_{\mu\nu}) \otimes \rho h_{\nu\gamma}(r_{\nu\gamma}), \quad (8)$$

and the HNC closure is written as

$$g_{\alpha\gamma}(r) = \exp\bigl(-\beta u_{\alpha\gamma}(r) + h_{\alpha\gamma}(r) - c_{\alpha\gamma}(r)\bigr), \quad (9)$$

where $h_{\alpha\gamma}$ and $c_{\alpha\gamma}$ are the site–site pair and direct correlation functions, respectively; $g_{\alpha\gamma} = h_{\alpha\gamma} + 1$ is the pair distribution function; $\omega_{\alpha\gamma}$ is the intramolecular correlation matrix; $\otimes$ denotes convolution in real space and summation over repeating indices; ρ is the liquid number density; and $\beta = 1/kT$ is the inverse temperature.

Solving RISM and HNC equations [(8) and (9)], we iterate $rc_{\alpha\gamma}(r)$ specified in real space rather than in a reciprocal one. First we obtain $h_{\alpha\gamma}(r)$ from the RISM eq. [(8)]. The convolutions in the latter are evaluated by the standard 1-D FFT on an exponential grid[19,20] in order to allow for a long-range asymptotic behavior due to Coulomb interactions. Then $g_{\alpha\gamma}(r)$ is calculated from the closure (9), and finally the residual is set up as

$$R_{\alpha\gamma}\bigl[\{c_{\alpha\gamma}(r)\}\bigr] = r\bigl(g_{\alpha\gamma}(r) - h_{\alpha\gamma}(r) - 1\bigr). \quad (10)$$

Unlike the conventional approach,[3–5] we do not renormalize the RISM and HNC equations explicitly. One can show the residual (10) as a function of $c_{\alpha\gamma}$ does not change on renormalization. The role of renormalization thus consists of correct treatment of the long-range asymptotics of the distribution functions, as well as specifying the initial guess of $c^{(0)}_{\alpha\gamma}(r)$ to be as close to the solution as possible. In particular, it is necessary to prevent overflow of the exponent in the HNC closure (9) in a region of strong attraction. The asymptotics of $c_{\alpha\gamma}(r)$ are determined for a polar molecule mainly by the Coulomb site–site potential forming a deep attractive well and a long-range tail. On the other hand, $c_{\alpha\gamma}(r)$ tends to a constant as $r \to 0$. Therefore, we start the iteration with

$$c^{(0)}_{\alpha\gamma}(r) = -\beta q_\alpha q_\gamma \frac{1 - \exp(-\sigma r)}{r}, \quad (11)$$

where σ is a parameter. Taking into account the Lennard–Jones (LJ) interaction has a negligible effect so it can be dropped. Notice that for a nonpolar molecule, one can simply put $c^{(0)}_{\alpha\gamma}(r) = 0$. Another choice of the initial vector involves the error function[16] rather than the exponent.

Special care should be taken in calculation of the forward Fourier transform of the site–site direct correlation function $c_{\alpha\gamma}(r)$. Because of the presence of the Coulomb site–site potentials, it diverges as $k \to 0$. A term with the Coulomb long-range asymptotics is separated out, handled analytically, and then added back,[21]

$$c_{\alpha\gamma}(r) = -\beta q_\alpha q_\gamma \frac{1 - \exp(-\sigma r)}{r} + c^{(s)}_{\alpha\gamma}(r),$$

$$c_{\alpha\gamma}(k) = -\beta q_\alpha q_\gamma \frac{4\pi\sigma^2}{k^2(k^2 + \sigma^2)} + c^{(s)}_{\alpha\gamma}(k),$$

whereas the remaining short-range part, $c^{(s)}_{\alpha\gamma}(r)$, is transformed numerically by using the nonlinear FFT.[19,20] It is obvious to use the analytical term of the same form as in (11) because of its simple Fourier transform. The backward nonlinear FFT of $h_{\alpha\gamma}(k)$ creates no difficulty because it does not have the Coulomb asymptotics.

Employing the initial guess (11), we avoid the procedures of sequential solution of the equation at gradually decreasing temperature (the so-called cooling) and increasing site charges (charging), which are usually employed to facilitate convergence.[3–18] This greatly reduces computation time.

3-D RISM and HNC Equations

The modified DIIS method appears to be especially useful in calculation of a 3-D liquid structure. Here we use it to calculate 3-D site profiles of a pure molecular liquid around one of its molecule treated as a central particle. To obtain the 3-D RISM equation for the above 3–D profiles, we regard the central molecule as a single ''solute'' of arbitrary shape and generalize the solute–solvent RISM equation at infinite dilution to the 3-D case.[7] It has the form

$$h_\gamma(\mathbf{r}_\gamma) = c_\alpha(\mathbf{r}_\alpha) \otimes \bigl(\omega_{\alpha\gamma}(r_{\alpha\gamma}) + \rho h_{\alpha\gamma}(r_{\alpha\gamma})\bigr), \quad (12)$$

where $h_\gamma(\mathbf{r})$ and $c_\gamma(\mathbf{r})$ are, respectively, the correlation function and the direct correlation function of the solute specified on a 3-D grid in a periodic box and $h_{\alpha\gamma}(r)$ is the radial site–site pair correlation function of the solvent. The derivation of this equation is presented in detail elsewhere.[22] As distinct from ref. 7, in the present work we obtain the pair correlation function between sites α and γ self-consistently by averaging the 3-D correlation profile of site γ over the orientation $\Omega_{\alpha\gamma}$ of the vector $\mathbf{r}_{\alpha\gamma}$ at fixed separation $r_{\alpha\gamma}$ from site α,

$$h_{\alpha\gamma}(r_{\alpha\gamma}) = \Omega_{\alpha\gamma}^{-1} \int d\Omega_{\alpha\gamma}\, h_\gamma(\mathbf{r}_\gamma). \qquad (13)$$

The convolution in (12) is calculated by using the 3-D FFT technique.[23] Unlike the 1-D case, the 3-D FFT is applied directly to the whole function $c_\gamma(\mathbf{r})$. For a polar but electroneutral solute, $c_\gamma(\mathbf{r})$ has a dipole or higher multipole long-range asymptotics rather than a Coulomb one and so is free from the singularity at $k = 0$. Moreover, a charged solute is handled by applying a compensating background charge and forcing the whole supercell to be electroneutral. This is necessary in the Ewald summation of Coulomb interactions in a supercell and is usually assumed in computer simulation of liquids.[24] The initial Coulomb potential of a single charged solute is thus screened by the background charge at a length of box size. Therefore, the box should be big enough to include the region of significant change in the solvent density around the solute.

The 3-D generalization of the HNC closure that we used is written as

$$g_\gamma(\mathbf{r}) = \exp\bigl(-\beta u_\gamma(\mathbf{r}) + h_\gamma(\mathbf{r}) - c_\gamma(\mathbf{r})\bigr). \qquad (14)$$

It should be noted that other versions of the HNC closure are possible with orientational averaging of the exponent function of a part of the site potential $u_\gamma(\mathbf{r})$.[6,22]

The 3-D RISM equations [(12) and (13)] are similar to the molecule-site OZ (MSOZ) approach developed recently for a one-component molecular fluid.[6] The difference is that, instead of the 3-D distribution profiles, the latter averages the 3-D direct correlation functions, $c_\gamma(\mathbf{r})$. However, this seems to be more tedious because the direct correlation $c_\gamma(\mathbf{r})$ has the long-range dipole asymptotics of the initial potential, whereas the screened interaction, $h_\gamma(\mathbf{r})$, decays much faster.

We carry out the orientational averaging (13) by applying it to the Fourier expansion of $h_\gamma(\mathbf{r})$ in 3-D plane waves, which in this case reduces to that in spherical waves,

$$h_{\alpha\gamma}(r) = \Omega_{\alpha\gamma}^{-1} \int d\Omega_{\alpha\gamma} \sum_k h_\gamma(\mathbf{k}) \exp(-i\mathbf{k}\cdot\mathbf{r}_\gamma)$$

$$= \sum_k \frac{\sin(kr)}{kr} \sum_{|\mathbf{k}|=k} \exp(i\mathbf{k}\cdot\mathbf{r}_\alpha) h_\gamma(\mathbf{k}), \quad (15)$$

where $\exp(i\mathbf{k}\cdot\mathbf{r}_\alpha)$ is the phase factor due to shift of the center of averaging from the origin to site α. The orientational averaging procedure thus consists of performing the 3-D FFT, summing the expansion coefficients with equal absolute values of wave vector $\mathbf{k}$, and then synthesizing $h_{\alpha\gamma}(r)$ of spherical waves on a linear 1-D radial grid. Finally, the radial distribution function are transformed by the linear 1-D FFT and then splined to obtain $h_{\alpha\gamma}(k)$ at wave vector absolute values k necessary for 3-D convolution in (12). The parameters of the 1-D grid are chosen in such a way as to override the resolution of the 3-D grid in real and reciprocal spaces. The $h_{\alpha\gamma}(r)$ are calculated by (15) inside a sphere, $r < L_{\max}/2$, with a diameter as big as the maximal box size, $L_{\max}$, and are padded with zeros outside it.

The above procedure of orientational averaging is substantially faster than the angular integration over a sphere by using Lebedev's quadrature employed in ref. 6. A shortcoming of (15) is that it introduces small oscillations of the averaged radial distribution function near the particle core edge, which touches the negative region. However, this is of no importance because they are smoothed out in convolution in (12). We checked the averaging procedure (15) against the explicit integration of the 3-D profiles over the orientations by interpolating the profiles between the 3-D grid points and employing the 100-node Gauss quadrature for each of the angular spherical coordinates φ and $\cos\theta$. The difference in the resulting 3-D profiles, $h_\gamma(\mathbf{r})$, for using these two ways of orientational averaging in the process of solution of the 3-D RISM and HNC equations is negligible. The 1-D site–site pair distribution functions, $g_{\alpha\gamma}(r)$, can be refined at the end by applying the latter averaging procedure once.

We solve eqs. (12)–(14) for $t_\gamma(\mathbf{r}) = h_\gamma(\mathbf{r}) - c_\gamma(\mathbf{r})$. Inserted into the HNC closure (14), it yields g_γ and then c_γ. Thereafter we average g_γ by (13) to

obtain radial $h_{\alpha\gamma}$, and finally calculate h_γ from the RISM equation [(12)] to set up the residual $R_\gamma(\mathbf{r})$:

$$g_\gamma(\mathbf{r}_\gamma) = \exp\bigl(-\beta u_\gamma(\mathbf{r}_\gamma) = t_\gamma(\mathbf{r}_\gamma)\bigr),$$

$$h_{\alpha\gamma}(r_{\alpha\gamma}) = \Omega_{\alpha\gamma}^{-1}\int d\Omega_{\alpha\gamma}\bigl(g_\gamma(\mathbf{r}_\gamma) - 1\bigr),$$

$$h_\gamma(\mathbf{r}_\gamma) = (g_\alpha(\mathbf{r}_\alpha) - 1 - t_\alpha(\mathbf{r}_\alpha)) \otimes \bigl(\omega_{\alpha\gamma}(r_{\alpha\gamma}) + \rho h_{\alpha\gamma}(r_{\alpha\gamma})\bigr),$$

$$R_\gamma\bigl[\{t_\gamma(\mathbf{r}_\gamma)\}\bigr] = g_\gamma(\mathbf{r}_\gamma) - h_\gamma(\mathbf{r}_\gamma) - 1. \quad (16)$$

Similar to the 1-D case, we need neither the renormalization nor the cooling and charging procedures. The starting vector $t_\gamma^{(0)}(\mathbf{r})$ is determined by the long-range asymptotics of $t_\gamma(\mathbf{r})$ that is just that of $c_\gamma(\mathbf{r})$ but of opposite sign. Including the LJ potential into the initial guess $t_\gamma^{(0)}$ or adding the renormalized bond to account in $t_\gamma^{(0)}$ for the other term, $h_\gamma^{(0)}$, have a negligible result. Therefore, we do not include them in $t_\gamma^{(0)}$. In the 3-D case, it appears to be more convenient to choose the starting vector proportional to the Coulomb potential of the molecule site charges, broadened by the Gaussian distribution to a half-width δ,

$$t_\gamma^{(0)}(\mathbf{r}) = \frac{\beta q_\gamma}{V_{\text{cell}}}\sum_{\alpha,\mathbf{k}} q_\alpha \frac{4\pi}{k^2}\exp\left(i\mathbf{k}\cdot(\mathbf{r}-\mathbf{r}_\alpha) - \frac{\delta^2 k^2}{4}\right). \quad (17)$$

This potential is evaluated auxiliarly when performing the Ewald summation[24] employed to calculate the electrostatic contribution of the solute to the periodic potential of the supercell, $u_\gamma(\mathbf{r})$. The short-range term of the Ewald sum, as well as the contribution to $u_\gamma(\mathbf{r})$ due to the LJ potential, are tabulated in the supercell in real space by summation over all the solute sites subject to the minimal image condition.[24]

Numerical Results

To test the MDIIS method, we considered water described within the simple point charge (SPC) model[25] that comprises one oxygen (O) and two hydrogen (H) sites creating the 12–6 LJ and Coulomb potentials. The site separations are $L_{\text{OH}} = 1.0$ A and $L_{\text{HH}} = 1.633$ A. The LJ diameter and energy minimum and the site charge are, respectively, $\sigma_{\text{O}} = 3.166$ Å, $\varepsilon_{\text{O}} = 1.08 \times 10^{-21}$ J, $q_{\text{O}} = -0.82e$ for oxygen, and $\sigma_{\text{H}} = 1.0$ Å, $\varepsilon_{\text{H}} = 3.79 \times 10^{-22}$ J, $q_{\text{H}} = +0.41e$ for hydrogen (e is the elementary charge). We carry out the calculations at the temperature $T = 298$ K and water numerical density $\rho = 0.3334$ Å^{-3}. The LJ parameters between unlike sites are determined from the Lorentz–Berthelot combination rules, $\sigma_{\alpha\gamma} = (\sigma_\alpha + \sigma_\gamma)/2$ and $\varepsilon_{\alpha\gamma} = (\varepsilon_\alpha\varepsilon_\gamma)^{1/2}$.

We performed the 1-D calculations for the RISM and HNC equation on the grid of 512 points exponentially spaced in the range from $r_{\min} = 0.01261$ to $r_{\max} = 794.7$ Å. In expression (11) for the starting vector, we assume the parameter value $\sigma = 2$ Å^{-1}.

Figure 1 presents the root mean square value of the residual (10) versus the number of iterations performed. It reveals great acceleration of convergence by the MDIIS method as compared to the Picard iteration and dynamic relaxation. In the calculation the parameters of the dynamic relaxation procedure[7] were adjusted for the best convergence rate. The MDIIS damping parameter in (6) was chosen to be $\eta = 0.8$. The convergence rate improves with an increase of the number m of MDIIS vectors. However, a further increase over $m = 10$ worsens the performance, because the DIIS matrix in (5) becomes ill conditioned. The maximal convergence rate takes place for smaller residuals in the region of quadratic convergence.

For the 3-D calculation we chose the grid of $64 \times 64 \times 64$ points in a cubic box of size 20 Å, which is sufficiently large to cover three solvation shells around the central molecule. The broadening parameter in (17) had the value $\delta = 1$ Å.

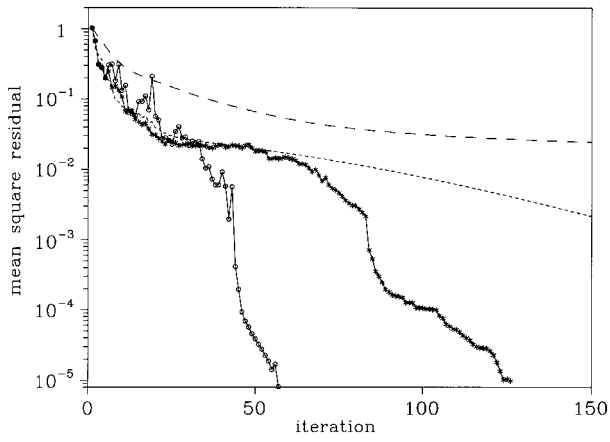

FIGURE 1. Root mean square residual against the number of iterational steps in calculation of the site–site pair distribution functions of the SPC water by the 1-D RISM and HNC equations. (—) The Picard iteration, (---) dynamic relaxation, and the MDIIS method with number of vectors (∗) $m = 3$ and (○) $m = 10$.

Figure 2 makes a comparison of the convergence rates in the 3-D case, depicting the root mean square magnitude of the residual (16). We found that here the optimal value of the MDIIS damping parameter is $\eta = 0.2$. Here the dynamic relaxation has a significant advantage over a plain iteration. However, the MDIIS procedure leads to crucial acceleration in the middle and final stages of the iterational process, even for a small number of iterated vectors constituting the iterative subspace ($m = 5$). When $m = 10$, it keeps the highest starting rate through all the run. A further increase of m does not result in improved performance due to the ill conditioning of the matrix in (5).

Notice that in both the calculations the MDIIS procedure was *not* restarted at any point of rise of the root mean square residual. We assume the MDIIS restarting threshold to be $K_r = 10$, which is sufficient for the MDIIS to ''try'' the residual behavior and to find the path to the solution without unnecessary restarts. It is clearly seen how the temporary rises are recovered by the significant drops in the residual magnitude at the following steps of the MDIIS procedure. However, our experience[26] shows that the restart of the MDIIS procedure occurs and is indeed necessary for successful and fast convergence in the case of strong nonlinearity for a highly charged solute in a polar solvent. A common feature of calculations for many systems is fast convergence at the beginning stage when the MDIIS procedure is ''figuring out'' a general behavior of the residual functions, then there is some slowing down or even oscillations in attempts to ''catch'' the solution, and finally there is a very fast convergence in the quadratic region.

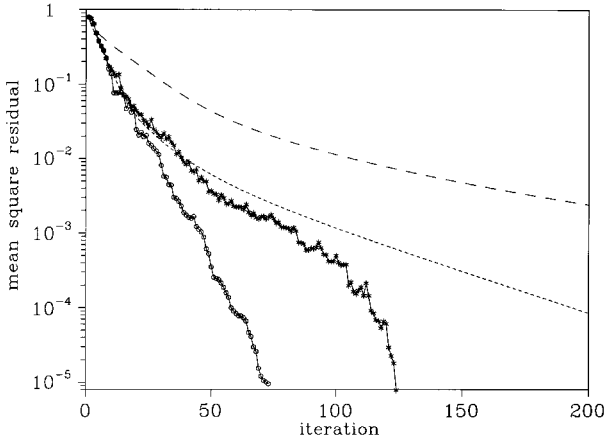

FIGURE 2. Root mean square residual against the number of iterational steps in calculation of the 3-D site distribution profiles of the SPC water around the central molecule by the 3-D RISM and HNC equations. (—) The Picard iteration, (---) dynamic relaxation, and the MDIIS method with number of vectors (∗) $m = 5$ and (○) $m = 10$.

The above-mentioned optimal values of the MDIIS damping parameter, η, obtained empirically and correspond to particular systems as discussed earlier. We observed that such values are typical for 1-D and 3-D systems. Besides, more nonlinear cases require smaller values of η.

In both the 1-D and 3-D cases considered, the overall convergence rate of the MDIIS method appears to be about 3–4 times higher than that of the combined MB + DIIS procedure applied to calculate the liquid of polar N_2-like molecules.[18] This is mainly due to the appropriate choice of the initial vector, allowing us to avoid the cooling and charging procedures, in spite of substantial nonlinearity peculiar to the case of strongly polar water molecules.

Figure 3 exhibits the 3-D distribution profiles of oxygen and hydrogen sites of the SPC water around the central molecule obtained by using the 3-D RISM and HNC equations. The profiles in the plane of the central molecule (Fig. 3a, b) and in the plane perpendicular to the molecule axis and containing its oxygen site (Fig. 3c, d) are shown. Notice the narrow high peaks of the oxygen and hydrogen profiles (Fig. 3a, b, d) corresponding to hydrogen bonding between water molecules.

The narrow peaks reveal that the bonds are strongly localized in front of the corresponding unlike sites. Bound oxygens are situated in two spots against the hydrogen sites of the central molecule (Fig. 3a). Bound hydrogens are located at the opposite site of the molecule in an arc passing around the oxygen site perpendicular to the molecule plane (Fig. 3b, d). The bonding positions (Fig. 3d) correspond to the tetrahedral configuration characteristic of hydrogen bonding of water molecules.

Because of the small hydrogen LJ radius, the peaks of the hydrogen profile split out from the first maximum and shift toward the oxygen site of the central molecule. At the same time, those of the oxygen profile remain within the first solvation shell because the hydrogens are located inside the oxygen LJ core.

The other peaks of the solvation shell of each site are located in the places of the maximal repulsion. The first and second peaks are higher and the oscillations are deeper in front of each of the sites. The four slight maxima of the first oxygen solvation shell (Fig. 3b) result from the neighbor hydro-

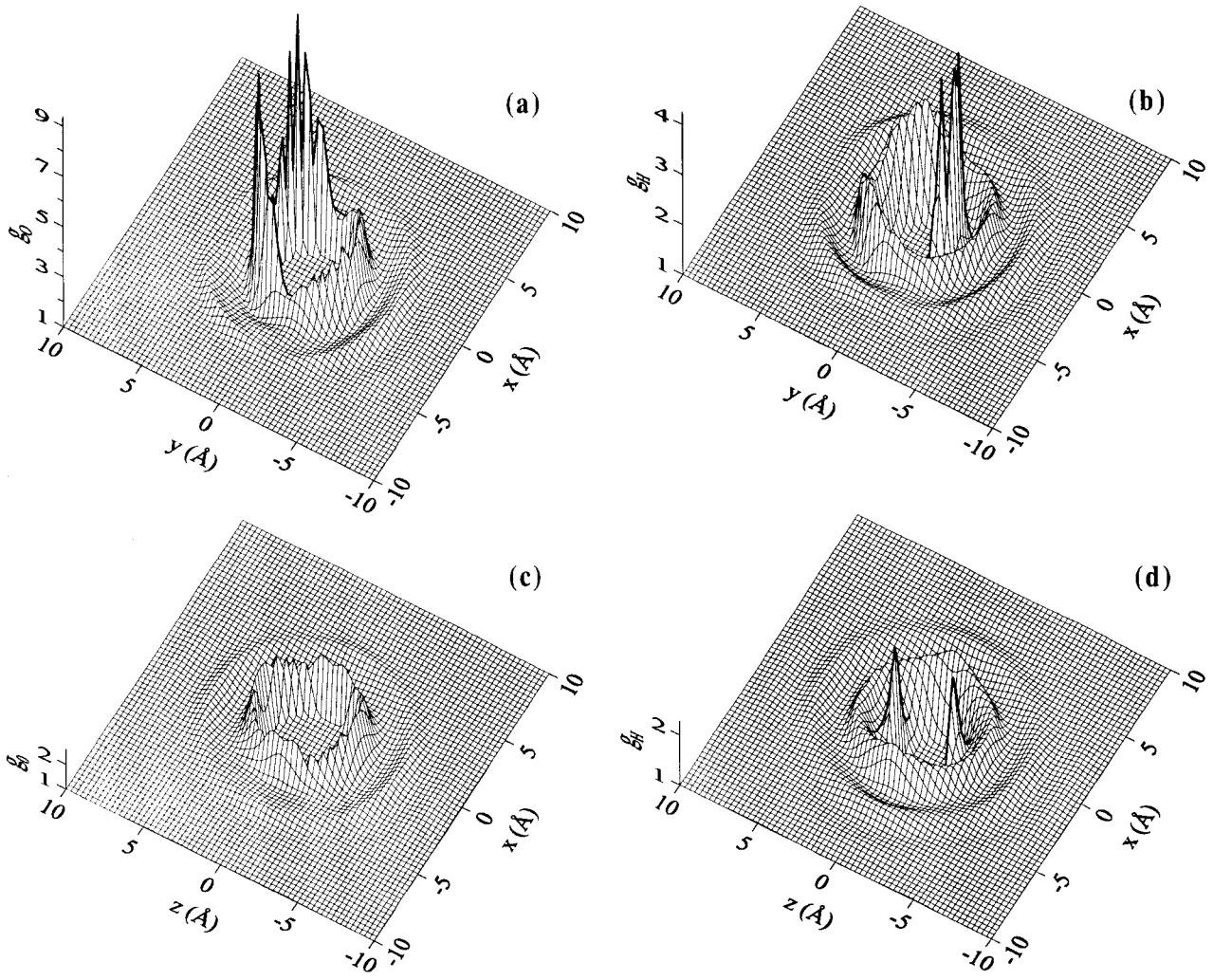

FIGURE 3. (a, c) Oxygen and (b, d) hydrogen site profiles of the SPC water around the central molecule (a, b) in the plane of the molecule and (c, d) in the plane perpendicular to the molecule axis and passing through the oxygen site. The hydrogen bonding peaks are traced with a bold line. The oxygen site is situated at the coordinate origin, $r = (0, 0, 0)$ Å, and the hydrogen sites are located at $r = (\pm 0.8165, 0.5773, 0)$ Å in the *XY* plane.

gens and thus reveal the tetrahedral symmetry of hydrogen bonding as well.

Finally, Figure 4 draws a comparison between the site–site pair distribution functions resulting from the 1-D RISM and HNC equations and those obtained by orientational averaging of the 3-D site profiles by using the 100-node Gauss quadratures at the end of the 3-D RISM and HNC calculation as described above. The former and latter 1-D results are close to each other. The difference between the radial distributions of hydrogen sites around the central molecule oxygen, g_{OH}, and oxygens around the central hydrogen, g_{HO}, is due to somewhat nonsymmetric treatment of the hydrogen bonds at different sites of the central molecule. This is because it is described at a 3-D level, which is different from 1-D for other water molecules. Notice that on orientational averaging the high narrow peaks of hydrogen bonding turn into the wider and shallower first peaks of the oxygen-hydrogen radial distributions.

Conclusion

We presented the modified method of DIIS that was applied to the integral equation theory of liquids to accelerate convergence of a solution of 3-D, as well as 1-D, equations. We updated the DIIS basis vectors at every iterative step by using

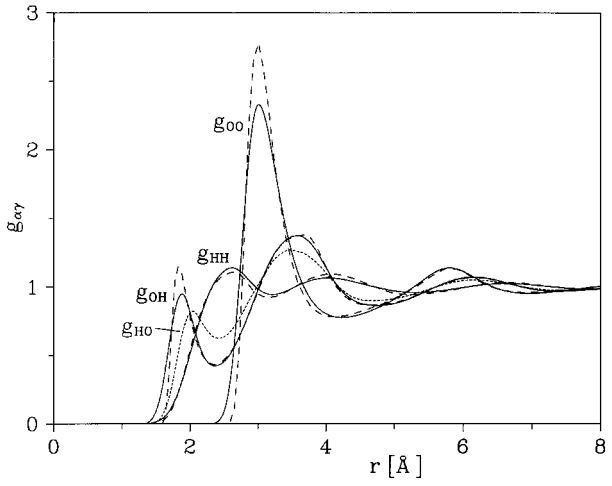

FIGURE 4. (—) and (---) SPC water radial distributions, $g_{\alpha\gamma}(r)$, obtained by averaging the 3-D profiles of site γ at a fixed separation from site α of the central molecule versus the (– – –) site–site pair distribution function resulting from the 1-D RISM and HNC equations.

the approximate residual obtained in the DIIS extrapolation. The MDIIS method provides great acceleration of convergence as compared to the Picard iteration and dynamic relaxation. This is of significant importance for time-consuming 3-D calculations.

We applied the method to solution of the 1-D RISM equation together with the HNC closure for a polar molecular liquid and to the 3-D generalizations of the RISM and HNC equations. We calculated and discussed the 3-D site distribution profiles of the SPC water model around one water molecule considered as a central particle.

In both the 1-D and 3-D cases, we perform iteration in real space. By the appropriate choice of the starting iterated vector, we avoid the procedures of sequential solution of the equations for gradually decreasing temperature (cooling) and increasing the site charges (charging). This significantly reduces computation time.

Acknowledgment

This work was supported by the Grant-in-Aid for Scientific Research on Priority Area of ''Electrochemistry of Ordered Interface,'' No. 09237265, from the Japanese Ministry of Education, Science, Sports, and Culture. A.K. is grateful to the Japanese Ministry of Education, for the support during his stay as a Visiting Professor at the Institute for Molecular Science.

References

1. Hansen J. P.; McDonald, I. R. Theory of Simple Liquids; Academic: London, 1976.
2. Chandler, D.; Andersen, H. C. J Chem Phys 1972, 57, 1930.
3. Hirata, F.; Rossky, P. J. Chem Phys Lett 1981, 83, 329.
4. Hirata, F.; Pettit, B. M.; Rossky, P. J. J Chem Phys 1982, 77, 509.
5. Hirata, F.; Rossky, P. J.; Pettit, B. M. J Chem Phys 1983, 78, 4133.
6. Cortis, C. M.; Rossky, P. J.; Friesner, R. A. J Chem Phys 1997, 107, 6400.
7. Kovalenko, A.; Hirata, F. Chem Phys Lett 1998, 290, 237.
8. Car, R.; Parrinello, M. In Simple Molecular Systems at Very High Density; Polian, A.; Lebouyre, P.; Boccara, N., Eds.; Plenum: New York, 1989; p 455.
9. Gillan, M. J. Mol Phys 1979, 38, 1781.
10. Labik, S.; Malijevsky, A.; Vonka, P. Mol Phys 1985, 56, 709.
11. Bérard, D. R.; Konoshita, M.; Ye, X.; Patey, G. N. J Chem Phys 1994, 101, 6271.
12. Kinoshita, M.; Okamoto, Y.; Hirata, F. J Chem Phys 1997, 107, 1586.
13. Pulay, P. Chem Phys Lett 1980, 73, 393.
14. Pulay, P. J Comput Chem 1982, 3, 556.
15. Hamilton, T. P.; Pulay, P. J Chem Phys 1986, 84, 5728.
16. Ng, K. J Chem Phys 1974, 61, 2680.
17. Maw, S.; Sato, H.; Ten-No, S.; Hirata, F. Chem Phys Lett 1997, 276, 20.
18. Kawata, M.; Cortis, C. M.; Friesner, R. A. J Chem Phys 1998, 108, 4426.
19. Talman, J. D. J Comput Phys 1978, 29, 35.
20. Rossky, P. J.; Friedman, H. L. J Chem Phys 1980, 72, 5694.
21. Kinoshita, M.; Hirata, F. J Chem Phys 1996, 104, 8807.
22. Kovalenko, A.; Hirata, F. J Chem Phys 1999, in press.
23. Press, W. H.; Flannery, B. P.; Teukolsky, S. A.; Vetterling, W. T. Numerical Recipes; Cambridge University Press: New York, 1986.
24. Allen, M. P.; Tildesley, D. J. Computer Simulation of Liquids; Oxford University Press: Oxford, UK, 1987.
25. Berendsen, H. J. C.; Postma, J. P. M.; von Gunsteren, W. F.; Hermans, J. In Intermolecular Forces; Pullman, B., Ed.; Reidel: Dordrecht, 1981.
26. Kovalenko, A.; Hirata, F. Unpublished manuscript.